# Statistical Downscaling for Precipitation Projections in West Africa

**Andrew Polasky** ( adp29@psu.edu )
Pennsylvania State University
**Jenni L. Evans**
Pennsylvania State University
**Jose D. Fuentes**
Pennsylvania State University

**Research Article**

**Keywords:** Climate Change, West Africa, Downscaling, Self-Organizing Maps

**Posted Date:** February 14th, 2023

**DOI:** https://doi.org/10.21203/rs.3.rs-2570247/v1



**Additional Declarations:** No competing interests reported.

# Statistical Downscaling for Precipitation Projections in West Africa

Andrew Polasky[1], Jenni L. Evans[1,2*] and Jose D. Fuentes[1]

[1]Department of Meteorology and Atmospheric Science, The Pennsylvania State University, University Park, 16801, PA, USA.
[2]Institute for Computational and Data Sciences, The Pennsylvania State University, University Park, 16801, PA, USA.

*Corresponding author(s). E-mail(s): jle7@psu.edu;
Contributing authors: adp29@psu.edu; juf15@psu.edu;

**Abstract**

The West Africa region (5° to 20°N and 10°E to 20°W) is particularly vulnerable to climate change due to a combination of unique geographic features, meteorological conditions, and socio-economic factors. Drastic changes in precipitation (e.g., droughts or floods) in the region can have dramatic impacts on rain-fed agriculture, water availability, and disease risks for the region's population. Quantifying these risks requires localized climate projections at a higher resolution than is generally available from global climate models. Using Self-Organizing Maps, we produce station-based downscaled precipitation projections for medium and high-emission climate scenarios for this region. We find slight increases in precipitation in the coastal areas, and decreases in the interior Sahel region by an average of 10% by 2100 under the high greenhouse gas-emission scenario of Shared Socioeconomic Pathway 5-8.5. Precipitation decreases in the Sahel are primarily driven by reductions in the number of rainy days during the wet season, rather than by consistent decreases in the magnitude of the precipitation amounts or decreases in the average length of the wet season.

**Keywords:** Climate Change, West Africa, Downscaling, Self-Organizing Maps

# 1 Introduction

Sub-Saharan Africa is home to more than one billion people, a number that is projected to double by 2050 (World Bank, 2020). The Intergovernmental Panel on Climate Change (IPCC) identifies Africa as one of the most vulnerable regions to climate change (Niang et al, 2014). This vulnerability is due to both large risks due to climate change, including increasing water stress, reduced crop yields, and increased range and incidence of vector-borne diseases, as well as a limited ability of many individuals and government agencies in the region to adapt to the rapid forthcoming changes (Sultan and Gaetani, 2016). The confluence of these factors means understanding the impact of climate change at the local level in the region is imperative for the planning of adaptation strategies for a resilient future.

To fully quantify these risks, accurate, local projections of climate scenarios are needed. Statistical downscaling can provide a computationally efficient method for bridging the gap between the resolution of Global Circulation Models (GCMs) and the scale needed for understanding climate change impacts (Maraun et al, 2010). Regional downscaling for precipitation is of particular importance, given the large impacts of climate change on people and their livelihoods. However, most global-scale models do not accurately represent precipitation at local scales (Stephens et al, 2010; Sillmann et al, 2013; Koutroulis et al, 2016). These challenges are especially acute in West Africa, where GCMs are particularly poor in their representations of precipitation (Paeth et al, 2011; Diallo et al, 2012; Ajibola et al, 2020), as a result of the complex dynamics driving precipitation processes in the region. The combination of the West African Monsoon and African Easterly Jet (AEJ) creates a sharp north-south gradient in total precipitation, with the vast majority of precipitation occurring during the convectively active wet season (Cook, 1999). The combination

of poor representation and hi gh vulnerability to climate change make the West Africa region an especially important area for research focused on improving future climate projections.

Crop yields for the current principal crops in the region are expected to decrease with climate change, and the inter-annual variability is expected to increase, significantly reducing food security in the region (Paeth et al, 2008; Schlenker and Lobell, 2010; Ahmed et al, 2015). The vast majority of agriculture in the region is rain-fed (Ewansiha and Singh, 2006), meaning changes in the amount and timing of precipitation can significantly impact crop yields, threatening food security in the region (Sultan and Gaetani, 2016).

In addition to agricultural concerns, water availability (Lebel et al, 2009; Badou et al, 2018), flooding (Di Baldassarre et al, 2010; Maranan et al, 2019; Panthou et al, 2014), and mosquito-borne diseases (Parham and Michael, 2010; Ermert et al, 2011; Mera et al, 2014) will be affected by changes to precipitation in the region. Planning to adapt to all of these forthcoming changes will require accurate, localized projections for the climate-change driven changes to precipitation in the region. Given these factors, the goals for this research are:

- Determine what variables can be used to realistically represent the synoptic meteorology of this region, to provide a suitable basis for downscaling of precipitation in the study region.
- Develop station-based downscaled projections for the West Africa region.
- Project key climate changes, such as variations in the length of growing season and shifts in average precipitation in the region.

## 1.1 Climatology of West Africa

West Africa is bounded by the Atlantic Ocean to the south and west, and the Sahara Desert to the north. These factors combine with the movement of

the Inter-Tropical Convergence Zone (ITCZ) to form the African Monsoon, creating distinct wet and dry seasons across the region (Sultan and Janicot, 2003). For the Sudano-Sahel region, from approximately 7° to 15°N, the wet season runs from June to September, during the Northern Hemisphere boreal summer (Janicot et al, 2008; Thorncroft et al, 2011). During this period, the ITCZ shifts north of the Equator, and moves across this region. A primary rain band, located well south of the line of surface level convergence, shifts from over the Atlantic Ocean during the winter months, coming onshore in early April, before moving north, reaching its furthest extent around 10°N in late June or early July (Thorncroft et al, 2011; Nicholson, 2013). This band of heaviest precipitation shifts back across the region at the end of the wet season, creating a "double peak" pattern in the annual precipitation for the coastal region. Similar to Thorncroft et al (2011), we refer to a "Coastal phase" in May and June, when the precipitation is heaviest at the coast, and a "Sahelian phase" from July to September, when the heaviest rain occurs over the inland region.

In the southern part of West Africa, there is a distinct coastal climate, characterized by increased rainfall and more moderate temperatures (Nguyen et al, 2011). Rainfall in this region peaks twice throughout the year, with an initial peak between April and June, and a secondary, smaller peak in the fall (Nicholson, 1993; Issa Lélé and Lamb, 2010). There is a sharp north-to-south gradient in the amount of precipitation that falls across the region, with totals ranging from up to 2000 mm per year along the coast of the Gulf of Guinea, to near 0 mm about 1000 km north in the Sahara Desert (Fig 1).

The strong heating over the Sahara and the relative cool air to the south create a significant north-to-south temperature gradient. The resultant thermal wind balance creates the AEJ, a mid-level jet typically lying between 13°

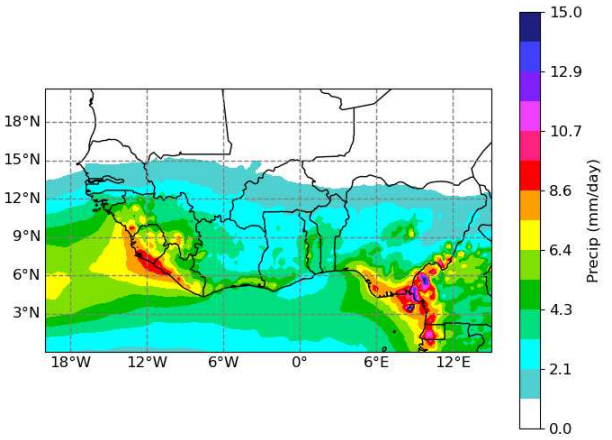


**Fig. 1** Average daily precipitation in the study region from the ERA5 reanalysis from 1979 to 2015.

and 17°N, and peaking around the 650 hPa level (Thorncroft and Blackburn, 1999). The AEJ is strongest during the summer months, when the temperature gradient is maximized by the heating of the Sahara. The AEJ supports the development of African Easterly Waves (AEWs), which play a significant role in development of convection in the region (Núñez Ocasio et al, 2020; Hamilton et al, 2020).

The AEWs are a critical synoptic feature in the region (Kiladis et al, 2006). These waves typically form over the highlands of Eastern Africa, and propagate along the AEJ through baroclinic-barotropic instability (Berry and Thorncroft, 2005; Thorncroft et al, 2008; Hamilton et al, 2020). Convection triggered by these waves produces a significant portion of the total precipitation in much of the region (Berg et al, 2013). Strong convection has also been shown to strengthen the waves, creating a feedback loop between the waves and the Mesoscale Convective Systems (MCSs) (Núñez Ocasio et al, 2020). Realistic downscaled climate projections, especially of precipitation, will require

predictors and methods that can capture the interactions between the AEWs and MCSs development.

In West Africa, MCSs are the primary driver of precipitation (Mathon et al, 2002; Lebel et al, 2003). As a result, the precipitation tends to come in large, concentrated bursts, rather than gradually distributed over many days. For the inland regions, nearly all of the annual precipitation falls during the wet season. MCSs are particularly important for extreme rainfall events, with the potential to cause serious flooding (e.g., Di Baldassarre et al (2010); Maranan et al (2019)). West African trends in rainfall indicate that precipitation events were decreasing in frequency, but increasing in intensity during the past 40 years (Panthou et al, 2014). Projecting the frequency of extreme rainfall events in future climates is necessary for developing strategies to cope with increased flooding risks in the region.

The topography of West Africa is mostly flat, with only moderate changes in elevation. The exception is the area around the Guinea Highlands, near the southwest coast of the study region. The highlands create an orographically enhanced rainfall maximum along the coast in this region (Fig. 1). Hamilton et al (2017) found that reductions in the size of the topography, such as those caused by moving to the coarse resolution of the GCMs, reduce the size of the precipitation maximum. Unfortunately, there is a paucity of station climate records in this region, so it is absent from our downscaling analysis (Fig. 2).

The region, particularly in the Sahel, is prone to extended periods of drought (Dai et al, 2004). From 1970 to 1990, the region on average experienced a decrease of rainfall between 20 and 30% compared to the preceding 30-year period (Lebel and Ali, 2009). This drought had dramatic consequences for those living in the region, causing shortened growing seasons, migration, and increased mortality (Mortimore, 2010).

## 1.2 Precipitation Projections for West Africa

Climate modeling in tropical regions poses significant challenges compared to the same task in the mid-latitudes. Weaker synoptic controls, increased frequency and strength of convection, and greater small-scale variability combine to produce patterns, especially of precipitation, that are not well described by global scale models (Crétat et al, 2014; Akinsanola et al, 2018). While the GCMs simulate many variables relevant to synoptic processes well, their representation of precipitation is generally poor. Downscaling can use the variables that are well simulated to better represent poorly simulated variables on the local scale and to project likely changes in future climate scenarios.

Regional dynamic downscaling, particularly on the scales required to adequately resolve mesoscale convection, is computationally expensive. Past dynamical downscaling efforts in the region of West Africa found improved characterization of precipitation compared to the direct GCM precipitation, running at a resolution of $0.44^\circ \times 0.44^\circ$ (Endris et al, 2013; Giorgi and Gutowski Jr, 2015; Dosio et al, 2015). However, this resolution is still too coarse to accurately capture convective-type precipitation, which produces the majority of rainfall in the region (Mathon et al, 2002). At coarse resolutions, past studies showed a wide range of projected changes across much of Africa, particularly in Central and West Africa, with many regional models disagreeing even on the sign of the changes (Vizy et al, 2013; Dosio et al, 2019, 2020). These differences raise significant uncertainties for the impacts of climate change on health, agriculture, and the development of tropical cyclones across Africa and the Tropical Atlantic.

Even in the higher resolution regional models, there were sizeable differences in the changes between the different GCMs used to drive the regional models, especially over West Africa (Dosio et al, 2019). This result indicates

that even higher resolution modeling is needed for accurately characterizing convective precipitation in the region. Statistical downscaling can fill this need without excessive computational requirements.

At the scale of GCMs, there has been limited improvement in precipitation projections in the tropics between Coupled Model Inter-comparison Project Phases 3 and 6 (CMIP3, CMIP6) (Fiedler et al, 2020), with large ranges in projections of temperature and precipitation in the West Africa region (Roehrig et al, 2013). These factors combine to create a challenging environment for statistical downscaling, which relies on the connections between the large scale features and the local conditions. In this study, we demonstrate that despite these challenges, statistical downscaling can still provide useful improvements to projections of precipitation in the region, and serve as a valuable tool for projecting the impacts of climate change in West Africa.

# 2 Data and Methods

## 2.1 Observational Data

Downscaling in West Africa is challenging due to the limited availability of long and continuous observational records across much of the region. The Global Summary of Day (GSOD) dataset provides daily observations for numerous stations across the region, but many of these stations have records too short to be used for statistical downscaling (National Climatic Data Center, 2020). To have a sufficiently larger number of stations, we use all stations with observation data for at least 5000 days between 1979 and 2014.

To ensure that the missing data do not bias the result (i.e., disproportionately missing rainy-season days would produce an average rainfall that was too low), the average temperature of the nearest reanalysis grid cell is compared

for the all days and those days with observations. Stations where the temperature averages are significantly different are excluded from the downscaling process. This process yields 84 stations spread across West Africa (Fig. 2). There are large areas with no stations that meet the criteria, but the stations are spread throughout the different climate regions of the study area. The lack of coverage limits the results of our downscaling to those areas where stations with suitable data are present.

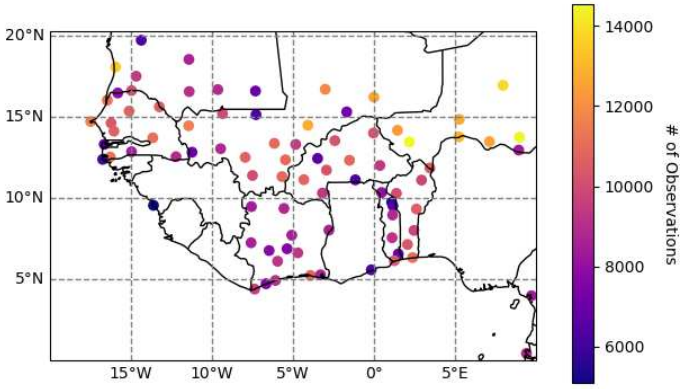


**Fig. 2** Locations of the 84 GSOD stations with at least 5000 daily observations of precipitation between 1979 and 2014 in West Africa. The number of daily observations available for each station is color coded.

## 2.2 Global Climate Data

Global reanalysis data from the European Centre for Medium-Range Weather Forecasts (ECMWF) Reanalysis v5 (ERA5) are used to train the downscaling models (Hersbach et al, 2020). The data are regridded using a bilinear process from the original 31 $\times$ 31 km$^2$ grid to a 1 degree $\times$ 1 degree to better match the resolution of the GCMs (Zhuang et al, 2020).

The GCM data sets are drawn from CMIP6. Eight models are chosen from a range of modeling centers, to provide an ensemble for use in exploring the future projections (Table 1). Where needed, outputs from each model are regridded from their original resolution using a bilinear process to a common 1-degree × 1-degree grid to perform the downscaling process (Zhuang et al, 2020).

**Table 1** List of CMIP6 models used for downscaling

| Model | Modelling Center | Horizontal Resolution | Vertical Levels |
|---|---|---|---|
| CESM2-WACCM | National Center for Atmospheric Research (USA) | 0.9x1.25 | 60 |
| EC-Earth3 | EC-Earth Consortium (Europe) | 0.7x0.7 | 91 |
| GFDL-CM4 | Geophysical Fluid Dynamics Laboratory (USA) | 1x1 | 33 |
| INM-CM5-0 | Russian Academy of Science (Russia) | 1.5x2 | 73 |
| IPSL-CM6A | Institut Pierre Simon Laplace (France) | 1.25x2.5 | 79 |
| MIROC6 | Japan Agency for Marine-Earth Science and Technology (Japan) | 1.4x1.4 | 81 |
| MPI-ESM1-2-HR | Max Planck Institute for Meteorology (Germany) | 0.94x0.94 | 95 |
| MPI-ESM1-2-LR | Max Planck Institute for Meteorology (Germany) | 1.8x1.8 | 47 |

The ERA5 and CMIP6 data are standardized as Z-scores. The CMIP6 values for the future periods are standardized using the mean and standard deviation values from the training period (1979-2006) to preserve the modeled climate changes. The data are also normalized by multiplying by the cosine of the latitude to account for differences in the size of grid boxes across the domain.

## 2.3 Downscaling Methods

We use the Self-Organizing Map (SOM) downscaling method introduced by Hewitson and Crane (2006) to downscale precipitation. This method has been used successfully for precipitation downscaling in other regions, including Florida (Sinha et al, 2018), the Midwest US (Polasky et al, 2021), and South Africa (Hewitson and Crane, 2006). The SOM method works by creating clusters of similar patterns of synoptic conditions, based on a training dataset. In this study, the training data set is drawn from the ERA5 for the period of 1979 to 2006. As the SOM is trained, it identifies a grid of patterns that cover the range of major weather types observed in the region. Using that trained grid, we compare each day in the CMIP6 projections to those synoptic patterns, and find the one that is most similar. Using that most similar pattern, we take the set of days in the training period matching the pattern, and sample from the distribution of precipitation values from those days to get a downscaled value for that day. A more complete description of the SOM method can be found in Polasky et al (2021).

In order to train the SOM method, we determine the size of the SOM grid using the quantization and topographical error (Kiviluoto, 1996). Identifying the "elbow" in grid size, while also minimizing the topographic error, we use $5 \times 7$ as the optimal grid size (Fig. 3).

## 2.4 Evaluation Metrics

We report changes to the precipitation-based ClimDEX indices for the region (Karl et al, 1999). These metrics provide a set of descriptive values to capture both amount and intensity of rainfall. A full list of the metrics and their definitions can be found in Table 5. In addition, we explore the changes to the length and timing of the wet season for the inland portions of the region. The

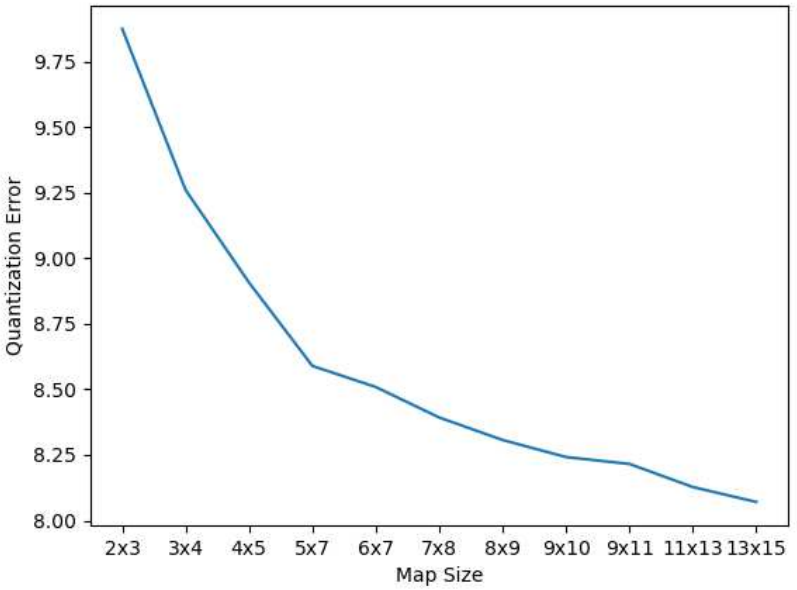


**Fig. 3** Quantization error for training SOMs of different sizes. Based on these results, identifying the elbow in quantization, we use a 5x7 grid for the final downscaling.

monsoon wet season, particularly in the semi-arid inland portions of the region, represents the key crop growing season (Stern et al, 1981; Akinseye et al, 2016). Predicting changes to the start and length of this season is therefore key for understanding climate impacts in this region.

Defining an objective standard for the start and end of the wet season is difficult, due to the nature of rainfall in much of the region, which tends to come in the form of large, semi-frequent MCSs, rather than more consistent daily precipitation events (Evans and Jaskiewicz, 2001; Mathon et al, 2002; Núñez Ocasio et al, 2020). A number of different criteria for defining wet seasons have been proposed, including absolute approaches using fixed precipitation values (Stern et al, 1981; Todorov, 1985), relative approaches based of a percentage of the rainfall at the location (Gregory, 1983; Liebmann et al, 2008), and more complex methods, factoring in additional factors, such as

**Table 2** ETCCDI ClimDEX Indices and definitions

| Index | Definition |
|---|---|
| TxMean | Average Daily Maximum Temperature |
| TxMin | Average Minimum Daily Maximum temperature per year |
| TxMax | Average Maximum daily maximum temperature per year |
| Su25 | Number of "Summer Days" above 25C |
| ID0 | Number of "Icing Days" where maximum temperature is below 0C |
| Tx90p | Days per year above the 90th percentile of maximum temperature in the training data |
| Tx10p | Days per year below the 10th percentile of maximum temperature in the training data |
| WSDI | Warm Spell Duration Index: The number of days with at least 6 consecutive days above t |
| TnMean | Average daily minimum temperature |
| TnMin | Average minimum daily minimum temperature per year |
| TnMax | Average maximum daily minimum temperature per year |
| Tn90p | Days per year above the 90th percentile of minimum temperature in the training data |
| Tn10p | Days per year below the 10th percentile of minimum temperature in the training data |
| CSDI | Cold Spell Duration Index: The number of days with at least 6 consecutive days below th |
| FD | Frost Days, number of days with minimum temperature below 0C |
| TR | Tropical Nights, number of days with minimum temperature above 20C |
| PrcpMean | Average precipitation per day |
| Rx1Day | Maximum 1-day precipitation |
| Rx5Day | Maximum consecutive 5-day precipitation |
| R95p | Annual Total Precipitation when daily rainfall is above the 95th percentile |
| R99p | Annual Total Precipitation when daily rainfall is above the 99th percentile |
| SDII | Simple Precipitation Intensity Index |
| CDD | Consecutive Dry Days, maximum length per year |
| CWD | Consecutive Wet Days, maximum length per year |
| R10mm | Days per year with precipitation above 10mm |
| R20mm | Days per year with precipitation above 20mm |

evapotranspiration (Hulme, 1987; Boyard-Micheau et al, 2013). In the interest of selecting a single and simple method that will work across the study region, we follow the method used by Liebmann et al (2008), based on the daily precipitation anomaly. An anomaly accumulation value (A) is calculated for each day of the year, using:

$$A(day) = \sum_{i=1}^{n} P_i - \overline{P} \tag{1}$$

Where $\overline{P}$ is the average daily precipitation, $P_i$ is the average precipitation on day i, and i is the day of the year. The wet season is then defined as the period between the minimum and maximum values of A throughout the year. Since the wet seasons in this region occur during the Northern Hemisphere summer, we use January $1^{st}$ to start the calculation of the anomaly accumulation.

# 3 Results

## 3.1 Downscaling Validation

We split the historical data into a training (1979-2006) and test (2007-2014) periods, in order to test the skill of the downscaling method on an independent data set. The SOM model is trained using the ERA5 reanalysis data for the training period, and then evaluated using both the reanalysis and GCM data for the test period.

### 3.1.1 Predictor Selection

Downscaling, particularly for precipitation, in West Africa is made more difficult by the complexity of the observed weather features in the region. The seasonal cycle of the region is dominated by the monsoon cycle, creating distinct wet and dry seasons across the region (Le Barbé et al, 2002; Xue et al, 2010; Nicholson, 2013). The monsoon, being a large scale circulation, can be easily seen on the scale of the climate models, in variables such as specific humidity and meridional wind (Fig. 4). These variables provide a useful basis for downscaling, as the circulation is both large enough to show up in the GCMs, and critical for determining the likelihood of precipitation.

Much of the precipitation in the region is convective in nature (Evans and Jaskiewicz, 2001). This precipitation occurs as small-scale convection along the coast, as well as larger and more organized MCSs further inland (Mathon et al, 2002; Núñez Ocasio et al, 2020). Due to their reliance on simulation of the strength of the boundary layer inversion, variables directly measuring the convective environment (i.e. convective available potential energy (CAPE) and Convective Inhibition (CIN)) are not skillfully predicted by the global models (Eden et al, 2012), limiting their utility in statistical downscaling approaches.

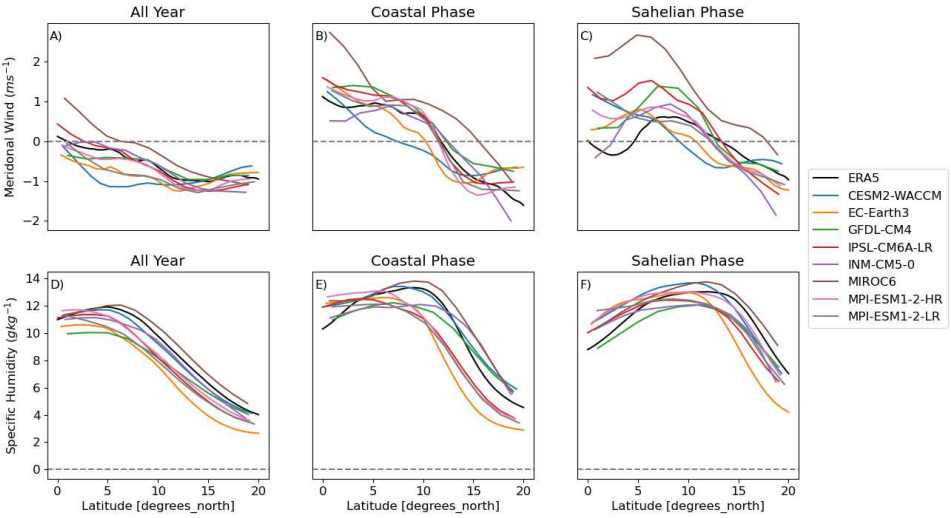


**Fig. 4** Averaged 850 hPa meridional wind (top) and specific humidity (bottom) for the full year, coastal monsoon phase (Late May - Late June), and Sahelian monsoon phase (July-September) for the ERA5 and CMIP6 models. In the Sahelian phase, particularly near the coast, there are sizeable differences between the ERA5 and CMIP6 models.

Selecting variables that serve as proxies for the commonly observed weather features, and are better represented in the global models, allows the downscaling methods to capture the range of synoptic conditions in the region, and produce more realistic distributions of events at the station level. To begin this process, we select a range of variables available in the reanalysis data, including temperature, wind components, vertical motion, geopotential height, and specific humidity at pressure levels from the surface to upper troposphere.

Of these variables, vertical motion should be a strong predictor of precipitation (Rose and Lin, 2003). However, especially in the tropics, the skill of the GCMs for vertical motion at the scales needed for local precipitation is limited (Rybka and Tost, 2014). We find a correlation between the ERA5 vertical motion and ERA5 precipitation, but not between the vertical motion and the station level precipitation, indicating that while the ERA5 reanalysis is internally consistent, the vertical motion variable does not represent the

station's reality to the extent, or on the scale, needed to predict observed precipitation. This result was borne out in testing downscaling models with and without vertical motion as a predictor, finding no improvement in skill when it was added as an input variable. Other variables, such as specific humidity, are generally better represented in the global scale models (Flato et al, 2014), and can still be used to represent the synoptic environment near the weather stations. These variables form the basis for our predictor set (Table 3).

From this set of variables, we train a number of SOM models using different sets of these predictors, and calculate the Probability Density Function Skill Score (PDFSS) across the 84 stations. The set of variables that perform best on this test and are selected for the final downscaling model are listed in Table 3. Using these predictors, we train a final SOM downscaling model on the ERA5 data, and evaluate it on the set of CMIP6 results provided by the chosen GCMs (Table 1).

**Table 3** Final set of predictors that are used for the downscaling. All variables are daily averages taken from the ERA5 and CMIP6 data, standardized as z-scores and cosine-normalized for use in the downscaling models.

| Variable | Pressure Level (hPa) |
|---|---|
| Temperature | 850 |
| Specific Humidity | 850, 500 |
| Meridional Wind | 850 |
| Zonal Wind | 700 |
| Sine of Day of Year | N/A |

### 3.1.2 Distribution Tests

To asses the skill of the downscaling models, we primarily use the PDFSS metric, which provides a non-parametric comparison of the similarity between two distributions (Perkins et al, 2007). The PDFSS is calculated using the formula:

$$S_{score} = \sum_{1}^{n} min(Z_m, Z_o) \tag{2}$$

where $S_{score}$ is the skill score, $Z_m$ and $Z_o$ are the observed and modeled frequency values falling in each bin used to calculate the PDF. The PDFSS provides a simple and interpretable metric for comparing climate statistics, where the focus is on recreating the distribution of events, rather then matching the individual weather events that are occurring on a specific day.

There is significant variation in the PDFSS across the stations used in this study. The largest single portion of this variability can be explained by the number of observations available for a given station (Fig. 5), with an $r^2$ value for the correlation between the number of observations and a station's skill score of 0.3. This result indicates that these methods would benefit from an increase in training data.

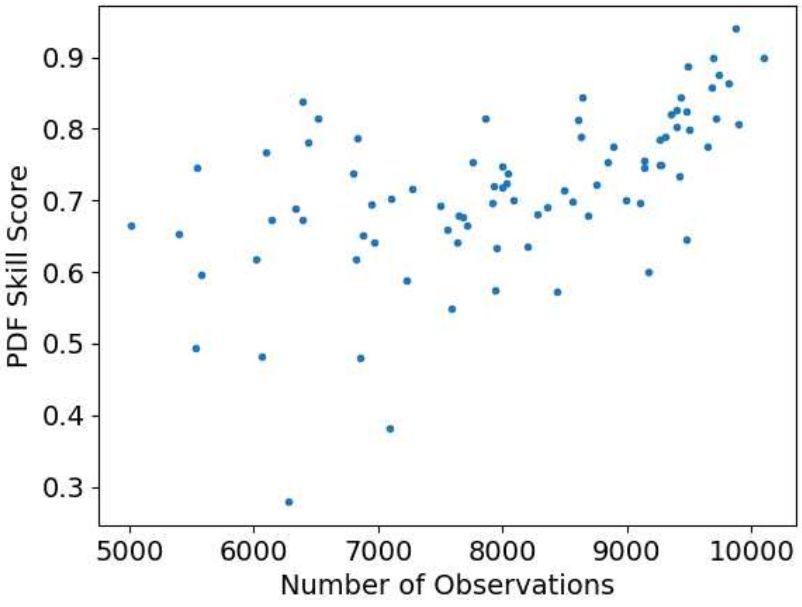


**Fig. 5** The PDFSS for the stations averaged across the eight CMIP6 models used for the downscaling for the test period. Downscaling skill increases with number of available observations.

### 3.1.3 Seasonality

An important test for the downscaling method is the ability to capture the seasonality of precipitation across the region, both to ensure that projections of changes to the seasons are well supported, and to check that the SOM is able to distinguish between weather patterns of different seasons. Plotting the average precipitation by the day of year for each individual station, we find that the downscaling does improve the representation of the seasonality, especially for inland stations (Fig. 6). However, for stations along the coast, the downscaling does not completely capture the dual-peak nature of the wet season or the decrease in precipitation as primary rain bands move further inland during the months of June, July, and August.

The downscaling based on the ERA5 data (Fig. 6, blue) provides superior results than the ones based on the CMIP6 GCMs (Fig. 6, red). Examining some of the key variables in the CMIP6 and ERA5 data, we detect some differences that help to explain the discrepancy. In particular, the 850 hPa meridional wind during the Sahelian phase of the monsoon shows a sign difference between the ERA5 data and the CMIP6 results between 0° and 7°N, in the region along the coastal boundary. The ERA5 data set has an average offshore flow at this level (850 hPa) during this stretch of time, while the CMIP6 values are mostly positive (Fig. 4c). This condition would have the effect of bringing more moist air in to the coastal region in the CMIP6 results. This assertion is supported by the generally higher values of specific humidity near the coast during this time period (Fig. 4f).

To assess the skill of the downscaling models across all the stations, we calculate the PDFSS for each station for the wet season, using the method for determining wet season described in Section 2.4 (Table 4). We define the coastal stations as those between 5° and 7 °N (10 stations), and the Sahel

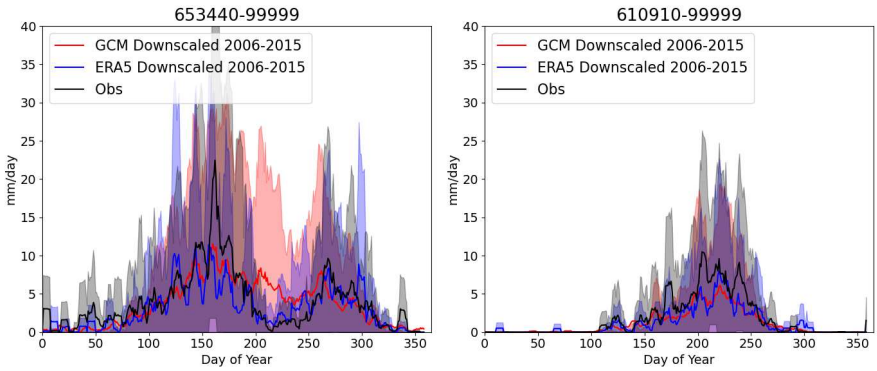


**Fig. 6** Average daily precipitation by day of year for a station near the coast (Cadjehoun , Benin), and one in the Sahel (Gaya, Niger). Observations (black), downscaled ERA5 (blue), and downscaled GCM (red) are shown for the test period of 2006-2015. For both stations, the downscaling of the reanalysis does a good job of capturing the seasonality of the observed precipitation, while the GCM downscaling struggles at the coastal station during the Sahelian phase of the monsoon.

stations are located between 8° and 15°N (44 stations). Downscaling skill is generally higher during the dry season, which is unsurprising, given that the variability in precipitation during that season is much lower. On average, results for the Sahel stations show higher skill than the ones for the coastal stations. The overall average skill score is pulled down by some lower skill stations near the edge of the region, especially in the South-East portion, in parts of Cameroon. The climatology of this region is quite different compared to most of the rest of the region, and would most likely require adjustments to the downscaling approach to produce reasonable skill in that region.

**Table 4** PDFSS by season for all 84 stations, Coastal stations (10) and Sahel stations (44). The wet season for each season is defined using the method described in section 2.4.

| | All Year | Wet Season | Dry Season |
|---|---|---|---|
| All Stations | 0.82 | 0.78 | 0.83 |
| Coast Stations | 0.84 | 0.81 | 0.84 |
| Sahel Stations | 0.86 | 0.82 | 0.85 |

### 3.1.4 SOM Patterns

The SOM method provides an opportunity to interrogate the areas where the downscaling generates results that do not realistically match the observed record. During the Sahelian phase of the Monsoon (July-September), the downscaled projections for the stations along the coast significantly overestimate the observed rainfall (Fig. 6). To understand the causes of this discrepancy, we plot the SOM heat map for this season for the ERA5 data, and for the results of each of the GCMs (Fig. 7). For the example station shown in Fig. 7, there is a consistent under-representation of SOM nodes in the upper left of the grid, including a number of nodes with low average precipitation values. The GCM downscaling shifts days away from these nodes, especially (0,1), (1,1), and (1,2), and over estimates the number of days in the lower left of the grid, such as nodes (0,5) and (1,5) during this season. When comparing the patterns associated with these nodes, the largest difference is observed for the specific humidity at the 500-hPa level, with the nodes in the upper left (with high frequency in the reanalysis) showing significantly drier conditions, especially in the southern portion of the study region (Fig. 8).

Comparing the specific humidity values between the ERA5 data and the GCMs during this season, we find a consistent pattern of the peak in the GCM specific humidity remaining too far to the south during these months (Fig. 9, right). One potential explanation is that the GCMs are producing an overabundance of vertical motion near the coast during this season, most likely due to a poorly resolved boundary layer inversion, leading to both increased precipitation and increased humidity at the 500-hPa level. This interpretation is consistent with the averaged vertical velocity over the region (Fig. 9, left) in the GCMs and ERA5 data. In particular, most of the GCMs show average ascent further south than is present in the reanalysis, indicating that

these models are over-representing convection near the coast. The GFDL-CM4 model provides more realistic results in moving the air ascent north during this season, and does the best of the GCMs used in this study at recreating the drop off in precipitation at the coastal stations during the Sahelian phase of the monsoon. If this is the root cause, the difference between the reanalysis and GCM data in specific humidity at the 500-hPa level is likely a symptom of the difficulties representing near-coast phenomena in GCMs. In particular, the parameterization of convection or the representation of sea-breeze interactions are areas that have been shown to have limited skill in GCMs (Eden et al, 2012; Stefanova et al, 2012; Birch et al, 2015).

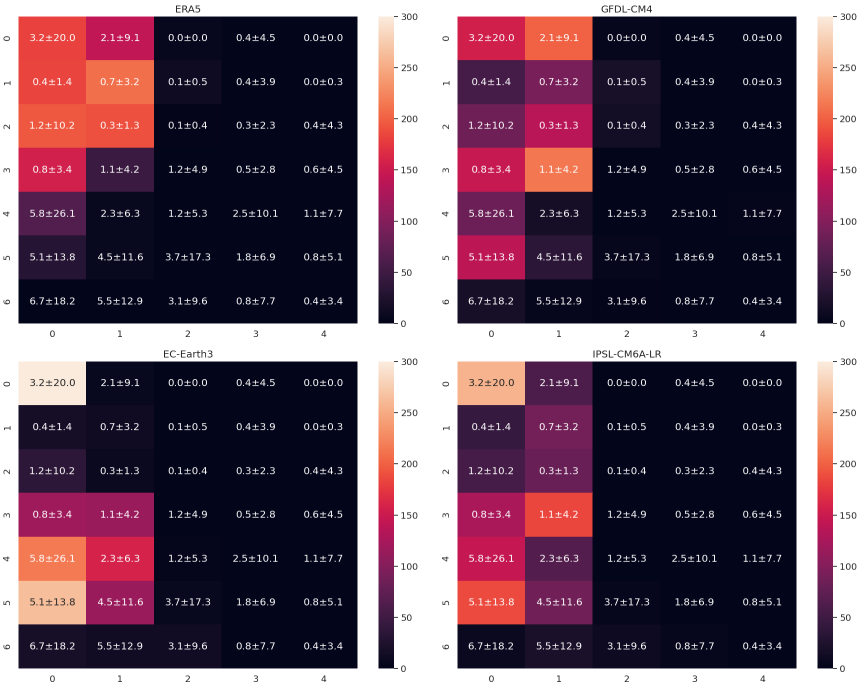


**Fig. 7** Heat map showing the frequency of each SOM node during the Sahelian monsoon phase in the historical period for the ERA5 reanalysis, and three selected CMIP6 models for an example station along the coast (Kotoka Airport, Accra, Ghana). The annotation on each node of the heat map is the mean and standard deviation of precipitation for the observed days that fall on that SOM node. The GCMs tend to have fewer days in the upper left, and more in the lower left of the map, than the reanalysis. The remaining CMIP6 models can be found in appendix A.

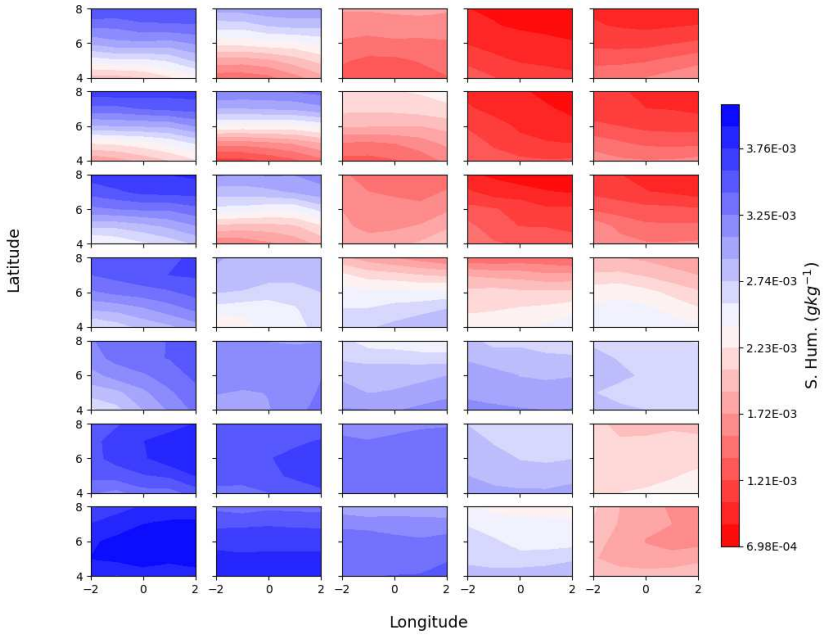


**Fig. 8** The pattern of 500 hPa specific humidity in the region around the same example station as in Fig. 7. The upper left nodes (under represented in the GCMs) show a significant area of drying to the south of the region compared to the lower left nodes (over represented in the GCMs). This indicates that the GCMs are not accurately capturing the changes in mid-level moisture during the inland phase of the monsoon, leading to the over-production of precipitation in both the GCM and the downscaling.

## 3.2 Projections of Near- and Far-Future Scenarios

There is significant uncertainty around the effects of climate change on West Africa, particularly with regard to precipitation (Niang et al, 2014). Even relatively small differences to the monsoon circulation could result in large changes in the timing and the amount of precipitation in many parts of the study region. Projections for change in precipitation for the region in GCMs range from -30% to +30% (Sylla et al, 2016).

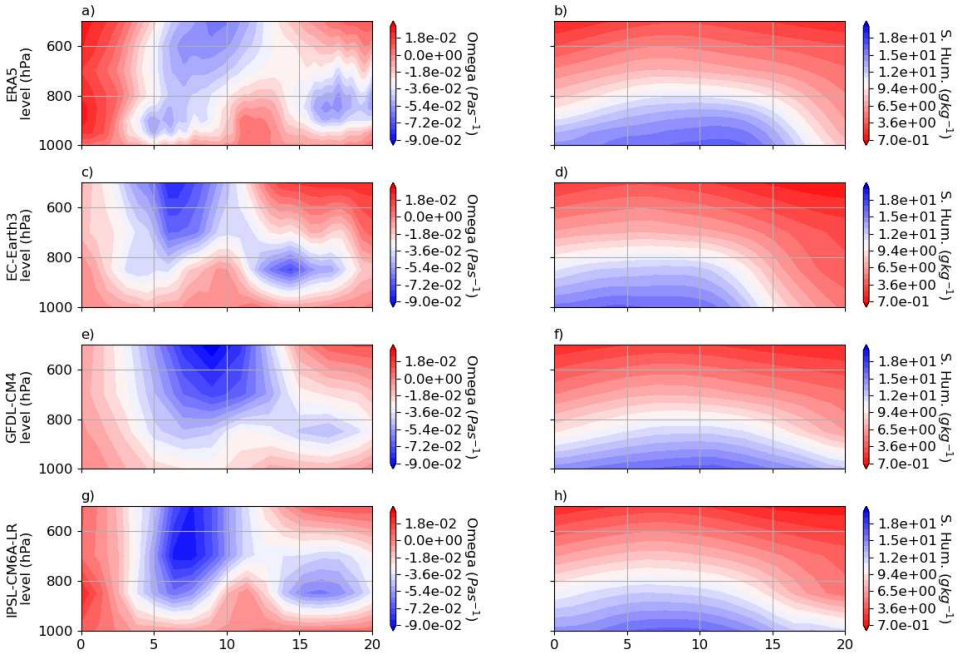


**Fig. 9** Zonal (10°E to 10°W) average vertical velocity (left) and specific humidity (right) for the wet season (June 1 to September 30) for the ERA5 reanalysis (a,b), and three selected global models. The GFDL-CM4 (e,f) model does the best job of the three at moving the core of the upward motion north of the coast (located around 5N).

We explore two contrasting scenarios from the Shared Socio-Economic Pathways (SSP), SSP2-4.5 and SSP5-8.5 (Gidden et al, 2019). The first scenario, SSP2-4.5, has global emissions peaking by 2050 then declining, leading to a global average temperature increase of 2.5-3.0°C by 2100. The SSP5-8.5 scenario represents high fossil-fuel use with emissions continuing to rise throughout the century, and temperatures increasing by 4.5-5.0°C by 2100 (Gidden et al, 2019). With these two scenarios, we project changes for two periods, near future (2021-2050) and far future (2071-2100).

Overall, averaging across all the stations in the study region, we find a decrease in the number of days with precipitation. This decrease is accompanied by a small decrease in the Simple Precipitation Intensity Index (SDII), indicating that the average amount of precipitation per rainy day is decreasing (Table 5, row 6) for both scenarios. These two effects combine to produce a decrease in the overall average precipitation decreasing, with the bulk of the change coming from the decrease in the rainy days. Breaking out the results by region, we find that precipitation will generally decrease in the central latitudes of the region (roughly 8-15°N), with average precipitation falling from 1.78 mm day$^{-1}$ in the historical period to 1.65 mm day$^{-1}$ in the far future period under the SSP 5-8.5 scenario (Fig. 10). For the same scenario, precipitation increases along the coast (from 2.87 to 3.06 mm day$^{-1}$) and in the northernmost extent of the region (from 0.49 to 0.71 mm day$^{-1}$) (Fig. 10). This pattern appears generally consistent in both the near future and far future periods, though the magnitude of the changes in the near future are relatively small.

**Table 5** ClimDEX indices averaged over the 84 stations, and over all years in each period. There is an overall decrease in average precipitation in the far future period, which is more pronounced in the SSP5-8.5 scenario (rightmost column).

| Index | Hist Obs | Test Obs | Hist Down-scaled | Test Down-scaled | Near SSP2-4.5 | Far SSP2-4.5 | Near SSP5-8.5 |
|---|---|---|---|---|---|---|---|
| Mean | 1.99 | 2.41 | 1.83 | 1.87 | 1.79 | 1.45 | 1.88 |
| Rx1day | 85.02 | 83.76 | 82.82 | 83.43 | 83.45 | 75.35 | 82.39 |
| Rx5day | 107. | 119.39 | 115.6 | 117.21 | 113.69 | 99.68 | 114.53 |
| R95p | 80.43 | 69.43 | 69.35 | 68.23 | 70.35 | 69 | 69.17 |
| R99p | 150.37 | 114.22 | 116.9 | 112.1 | 120.26 | 117.5 | 119.06 |
| SDII | 13.3 | 12.49 | 12.35 | 12.27 | 12.43 | 12.02 | 12.38 |
| CDD | 50.59 | 60.71 | 90.38 | 87.84 | 89.76 | 95.72 | 92.38 |
| CWD | 1.42 | 1.53 | 1.13 | 1.1 | 1.11 | 1.09 | 1.12 |
| R10mm | 15.88 | 21.31 | 20.01 | 20.55 | 18.99 | 15.46 | 20.3 |
| R20mm | 9.16 | 12.52 | 11.03 | 11.34 | 10.5 | 8.46 | 11.17 |

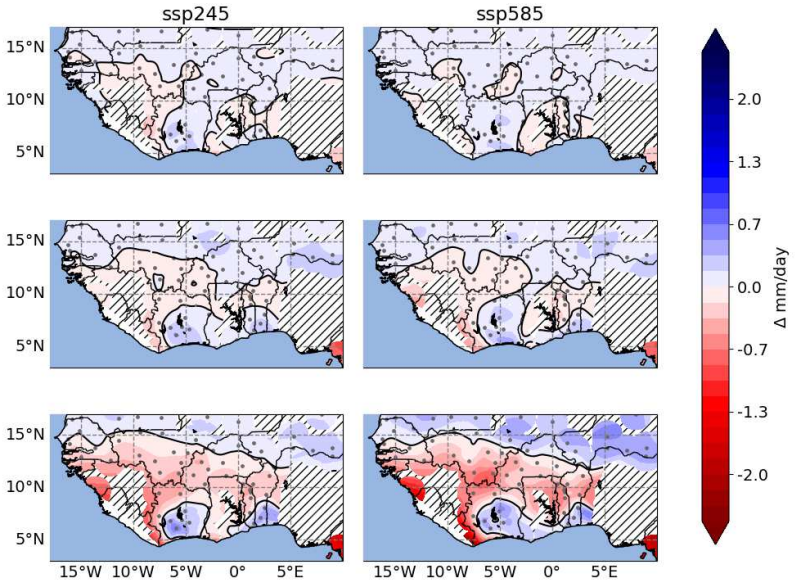


**Fig. 10** Change in precipitation between the training period and test (top), near (middle), far(bottom) periods for the two climate scenarios, averaged over the eight CMIP6 models. Hatched area represents areas greater than 150km from a downscaling station, which are excluded from our analysis. By the far future period, we see a more consistent pattern emerge, with increased precipitation along the coast and in the far north of the region, with decreased precipitation in the central portion of the region.

### 3.2.1 Change in Wet Season

One potentially important feature for climate projections for the region is the length of the wet season, especially in the semi-arid Sahel region. The rainy period provides the primary growing season for crops, and recharges aquifers, rivers, and hydrological basins, providing the water resources for the dry season. Currently, this season typically runs from late June through September. In both scenarios for the Sahel stations, our results indicate a shift to generally later dates for the wet season: with the average start date in the Sahel moving 8 days later under SSP2-4.5, and 15 days later under SSP5-8.5 in the far future period (Fig. 11). We generally see a decrease in the wet season length for the

region just to the north of the coast, then an increase in length for the central region, from about 10-15°N (Fig. 12). The delay is consistent with other studies of GCM projections, which have generally found a delayed start under warming climate scenarios (Biasutti and Sobel, 2009; Ibrahim et al, 2014). While we find a similar delay in the onset of the wet season, we do not see the corresponding decrease in the length of the wet season in the Sahel region. Rather, the wet season shifts later in the year, and on average increases in length by 7.8 days in for SSP2-4.5, and 5.2 days for SSP5-8.5 in the far future period.

In the Sahel, the form of the seasonal change of the wet season can be examined in more detail by analyzing the frequency or occurrence of the SOM nodes (Fig. 13). In the historical period, there is a distribution of days across the lower portions of the SOM map (rows 5 and 6 especially). In the far future period, we get a general decrease in frequency from some of the central nodes (e.g. 5,2 and 5,3), and increases in the lower left and lower right. These two areas represent lower precipitation (left, averaging 1.7 mm day$^{-1}$) and higher, more variable precipitation (right, averaging 9.8 mm day$^{-1}$) compared to the nodes with the largest decrease in frequency, which average 5.3 mm day$^{-1}$. These changes match what we see in the ClimDEX values for the Sahel stations, with a decrease of around 10% in the average precipitation (from 1.94 to 1.74mm day$^{-1}$), while metrics of extreme precipitation stay near constant (e.g., the 99$^{th}$ percentile goes from 110 to 113 mm). Coupled with Fig. 11, this result indicates fewer days with precipitation (from 55 to 47 days) despite the increase in the overall length of the wet season.

## 4 Summary and conclusions

Preparing for climate changes in West Africa will require accurate, local information on likely changes in precipitation amounts and intensity throughout

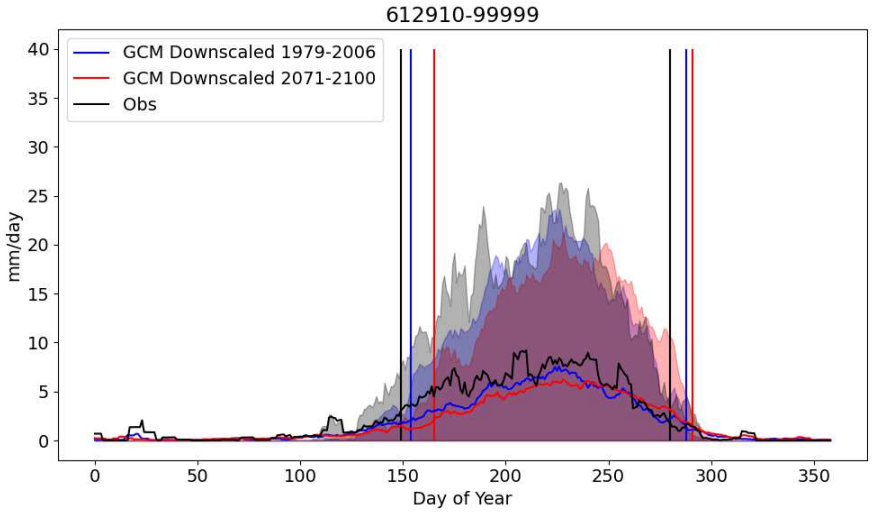


**Fig. 11** Average precipitation by day of year for an example station in the Sahel (Senou, Mali) for the observed (black), historical downscaled (dark blue), and far future period (light blue) under the SSP5-8.5 scenario. The vertical lines show the assessed start and end of the wet season, using the method described in section 2.4.

the region. The current generation of GCMs does not provide this information at the scales needed for many adaptation decisions such as predictions of crop yields and flooding potential. In this study, we demonstrate how SOM-based downscaling can be used to produce station-scale projections for climate change scenarios to provide the necessary downscaled data for modeling of important resources such as crops and water availability. While there are a limited number of available stations with long enough periods of record that can be used for statistical downscaling, there are enough to provide reliable estimates for much of the West Africa region, especially in the Sahel. The meteorology of West Africa poses several challenges for downscaling, due to the convective nature of the majority of the precipitation, and the poor representation of several key processes in the region in GCMs. Using the SOM method, we are able to identify areas where the GCMs are failing to capture the underlying dynamics, leading to significant errors in the projected precipitation. By

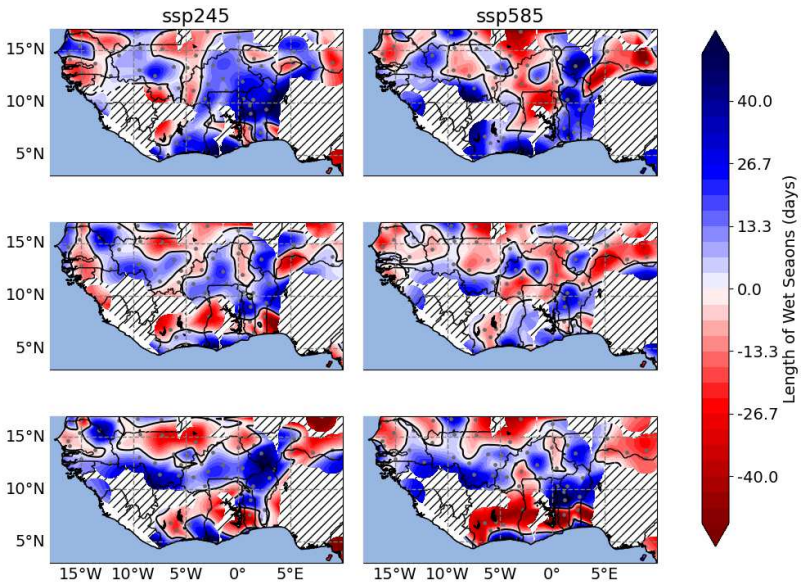


**Fig. 12** Difference in wet season length calculated for the historical period downscaling and the test (top), near future (middle), and far future (bottom) periods.

selecting variables that are both meteorologically relevant and better captured in the GCMs, we demonstrate that the SOM downscaling method can produce projections that capture a more realistic distribution of precipitation for the inland portions of the region, and greatly improve on the GCMs' precipitation. Near the coast, the SOM downscaling struggles to capture the seasonal variability as a result of differences between the GCM and ERA5 data, especially in the 500 hPa humidity values.

Using these methods, we project significant changes in precipitation distribution across the region in both emissions scenarios, with the largest signal in the SSP5-8.5 high-emission scenario. Along the south coast of West Africa, precipitation is likely to increase slightly, but these values are uncertain. In the Sahel, precipitation may decrease by an average of about 10% by the end of the

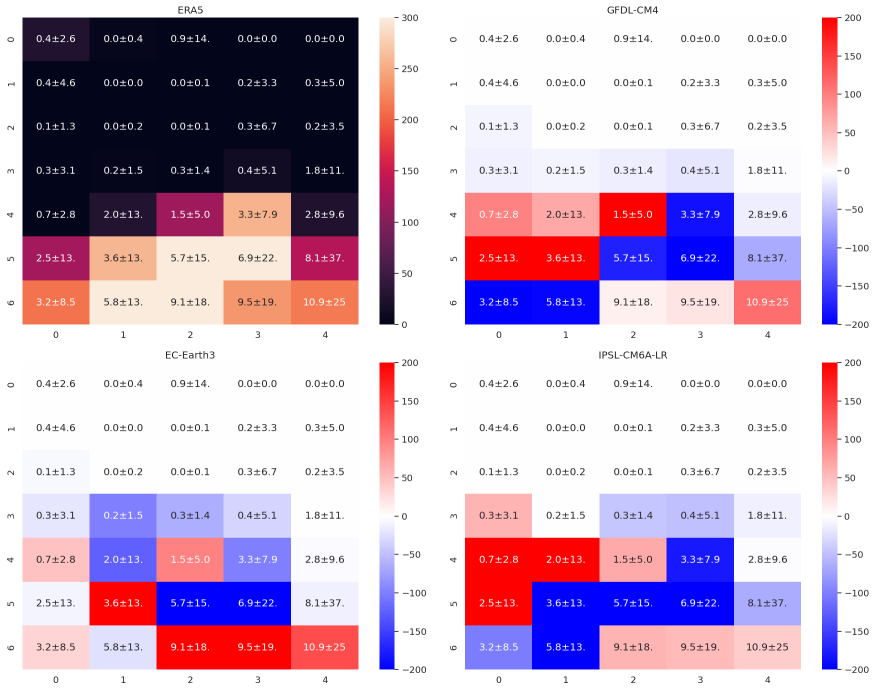


**Fig. 13** The difference in frequency of hits on each SOM node during the wet season for an example station located in the Sahel (Senou, Mali, same as in figure 11). The text within each SOM node represents the average and standard deviation of precipitation for historical days that fall on that node. The upper left panel shows the frequency for each node in the reanalysis for the training period, while each other panel shows the difference between the training and far future period under the SSP5-8.5 scenario for each respective model. Consistently across the models, there is a decrease in the nodes in the lower center of the SOM map, and a shift towards both right and left edges. This indicates a shift away from the more moderate monsoon precipitation days, and towards more dryer days (left) and extreme precipitation days (right).

century. This decrease in precipitation is driven by changes in the number of precipitation days, falling from 55 to 47 in an average year, while the frequency of extreme rainfall events stays close to constant. The decrease in precipitation in the Sahel is especially worrying, as this region is already frequently water stressed, and relies heavily on rain-fed agriculture.

These changes are likely to produce significant stressors for a region that is expected to see large increases in population during the coming century. Developing adaptation strategies for these forthcoming changes is an important step

to overcome the challenges created by climate change and thus create environmental resilience in the region. Planners in the region will need robust, localized projections for precipitation to address the challenges posed by the changing climate, especially with regards to agriculture and water management.

**Acknowledgments.** The US National Science Foundation funded the research under grant 1639342. Computations for this research were performed on the Pennsylvania State University's Institute for Computational and Data Sciences (ICDS) Roar supercomputer.

## Author Declarations

- Funding: This work was supported by the US Nation Science Foundation under grant 1639342
- Competing interests: The authors have no relevant financial or non-financial interests to disclose
- Ethics Approval: Not Applicable
- Consent to participate: Not Applicable
- Consent for publication: Not Applicable
- Data Availability: The data for this study was drawn from publicly available datasets which can be accessed at: ERA5 (https://www.ecmwf.int/en/forecasts/datasets/reanalysis-datasets/era5), CMIP6 (https://esgf-node.llnl.gov/search/cmip6/), GSOD (https://www.ncei.noaa.gov/access/metadata/landing-page/bin/iso?id=gov.noaa.ncdc:C00516)
- Code Availability: A streamlined version of the code used in this study can be found at: https://github.com/drewpolasky/CCdownscaling
- Authors' contributions: JE, JF, and AP contributed to study design and conception. Data collection, coding, and analysis was carried out by AP. The

first draft of the manuscript was written by AP, and all authors provided comments and edits. All authors read and approved the final manuscript.

# Appendix A Additional SOM Figures

In this appendix, we expand on the work that was done to determine the best input variables for the downscaling method, and to understand the what changes in the synoptic pattern contribute to the changes in the downscaling projection, as well as the patterns for the additional CMIP6 models used in the analysis (Figs. A1 and A2).


**Fig. A1** As in Fig. 7, but for all eight CMIP6 models, showing the frequency for each SOM node during the Sahelian phase of the monsoon for a coastal station Kotoka Airport, Accra, Ghana).

## A.1 Sahel

In the Sahel region, from roughly 8-15°N, the SOM downscaling is generally able to match the seasonality of the observed precipitation (Fig 6). In addition to determining the seasonality, the SOM also distinguishes between wet season days with low and high typical precipitation. Among SOM nodes with high frequency during the wet season, the average precipitation for the nodes ranges from 1.5 to 10.9 mm day$^{-1}$. This provides an indication that the downscaling is able to identify days likely to produce convective precipitation. Comparing those high and low precipitation SOM nodes, we find that the largest differences in the 850 hPa specific humidity, particularly to the north of the station (Fig. A3). In addition, there is a consistent pattern in the 700 hPa Zonal wind, where the higher precipitation days occur when the easterly wind is stronger to the north of the region, while on the lower precipitation days, the gradient is reversed (Fig. A4). This aligns with other studies of the role of the AEJ in the formation of MCSs, which provide much of the precipitation in the region (Thorncroft and Hoskins, 1994).

## A.2 Coast

Along the Coast of the region, we observe an inability for the downscaling to capture the seasonality of the precipitation (Sec. 3.1.3. In addition to the 500 hPa humidity discussed in that section, the meridional wind also reveals some aspects of where the GCMs are struggling to capture the key dynamics. During the Sahelian phase of the monsoon, we see the ERA5 reanalysis hitting a significant number of times on nodes (0,2) and (1,2), much more than in most of the GCMs (Fig. 7). In addition to the differences in 500 hPa specific humidity discussed in section 3.1.3, These nodes show a difference in 850 hPa meridonal wind, with the nodes that are over represented in the GCMs having

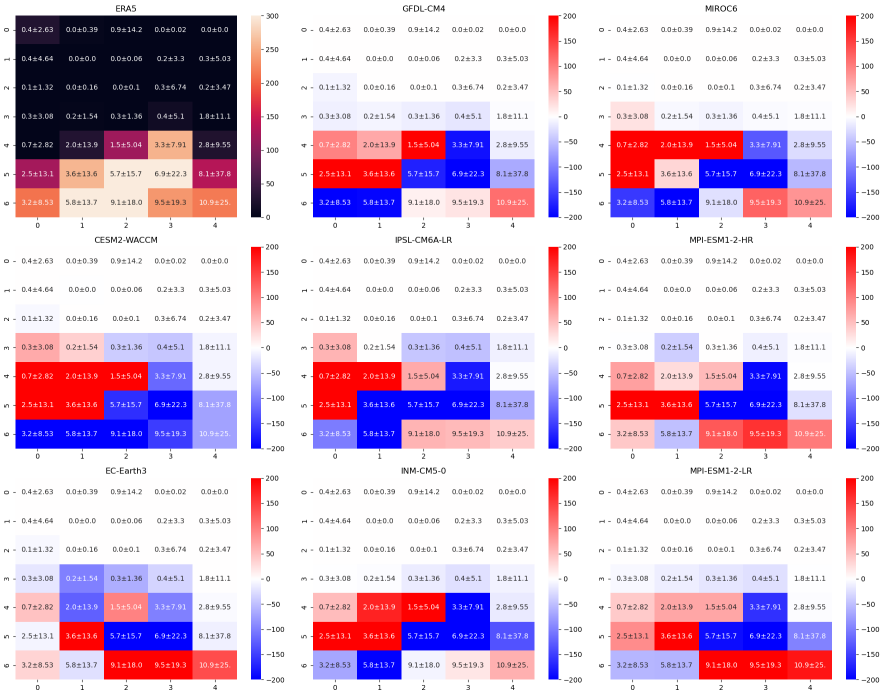


**Fig. A2** As in Fig. 8, but for all 8 CMIP6 models, showing the change in node frequency between the historical and far future period under the SSP5-8.5 scenario for a station in the Sahel (Senou, Mali).

a stronger southerly (onshore) flow (Fig. A5). This likely plays a role in the over-production of precipitation in the GCMs during this season, bringing in additional moisture and unstable air from the Gulf of Guinea.

# References

Ahmed KF, Wang G, Yu M, et al (2015) Potential impact of climate change on cereal crop yield in West Africa. Climatic Change 133(2):321–334

Ajibola FO, Zhou B, Tchalim Gnitou G, et al (2020) Evaluation of the performance of CMIP6 HighResMIP on West African precipitation. Atmosphere 11(10):1053

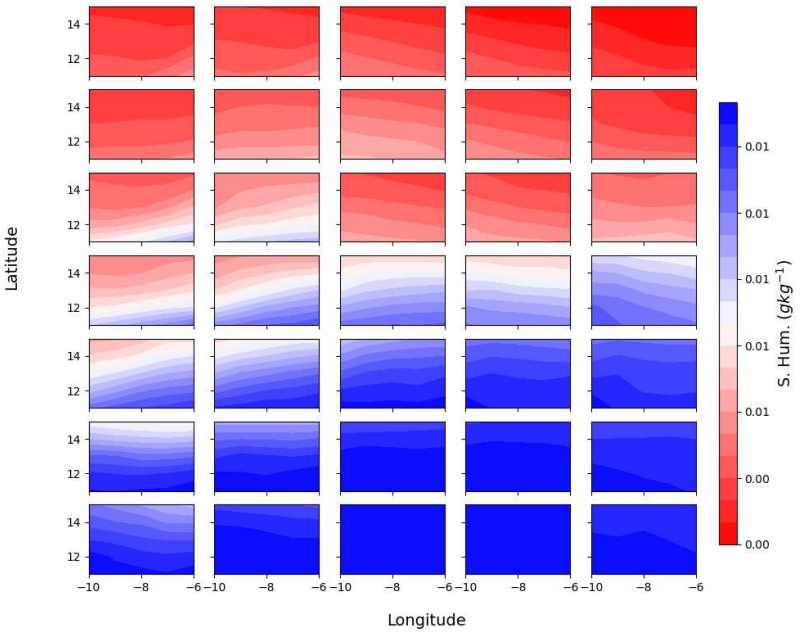


**Fig. A3** SOM nodes for 850 hPa specfic humidity near a Sahel station (Senou, Mali).

Akinsanola A, Ajayi V, Adejare A, et al (2018) Evaluation of rainfall simulations over West Africa in dynamically downscaled CMIP5 global circulation models. Theoretical and applied climatology 132(1-2):437–450

Akinseye FM, Agele SO, Traore P, et al (2016) Evaluation of the onset and length of growing season to define planting date—'a case study for Mali (West Africa)'. Theoretical and Applied Climatology 124(3):973–983

Badou DF, Diekkrüger B, Kapangaziwiri E, et al (2018) Modelling blue and green water availability under climate change in the Beninese Basin of the Niger River Basin, West Africa. Hydrological Processes 32(16):2526–2542

Berg A, de Noblet-Ducoudré N, Sultan B, et al (2013) Projections of climate change impacts on potential C4 crop productivity over tropical regions.

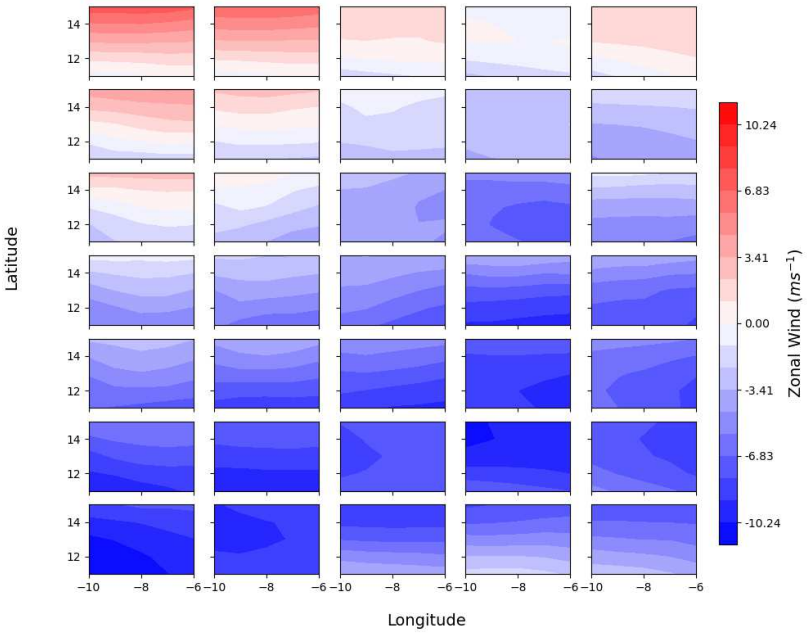


**Fig. A4** SOM nodes for 700 hPa Zonal wind near a Sahel station (Senou, Mali). This level was chosen to capture the AEJ, which typically peaks near the 600-700 hPa level.

Agricultural and Forest Meteorology 170:89–102

Berry GJ, Thorncroft C (2005) Case study of an intense African easterly wave. Monthly Weather Review 133(4):752–766

Biasutti M, Sobel AH (2009) Delayed Sahel rainfall and global seasonal cycle in a warmer climate. Geophysical Research Letters 36(23)

Birch CE, Roberts MJ, Garcia-Carreras L, et al (2015) Sea-breeze dynamics and convection initiation: The influence of convective parameterization in weather and climate model biases. Journal of Climate 28(20):8093–8108

Boyard-Micheau J, Camberlin P, Philippon N, et al (2013) Regional-scale rainy season onset detection: A new approach based on multivariate analysis.

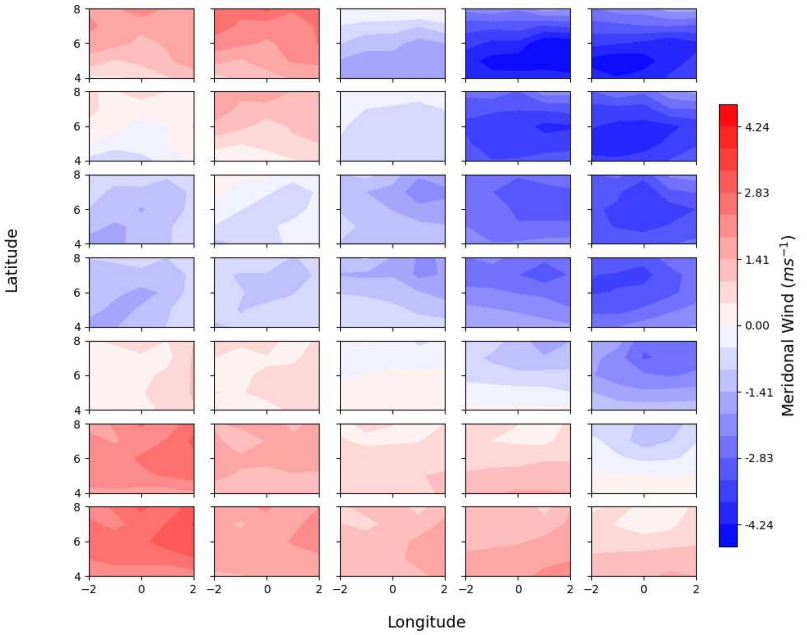


**Fig. A5** SOM nodes for 850 hPa meridional wind around a coastal station (Kotoka Airport, Accra, Ghana). The wet phase of the monsoon, corresponding to onshore (south) winds, primarily takes up the left and bottom parts of the grid.

Journal of Climate 26(22):8916–8928

Cook KH (1999) Generation of the African easterly jet and its role in determining West African precipitation. Journal of climate 12(5):1165–1184

Crétat J, Vizy EK, Cook KH (2014) How well are daily intense rainfall events captured by current climate models over Africa? Climate dynamics 42(9-10):2691–2711

Dai A, Lamb PJ, Trenberth KE, et al (2004) The recent Sahel drought is real. International Journal of Climatology: A Journal of the Royal Meteorological Society 24(11):1323–1331

Di Baldassarre G, Montanari A, Lins H, et al (2010) Flood fatalities in Africa: from diagnosis to mitigation. Geophysical Research Letters 37(22)

Diallo I, Sylla M, Giorgi F, et al (2012) Multimodel GCM-RCM ensemble-based projections of temperature and precipitation over West Africa for the early 21st century. International Journal of Geophysics 2012

Dosio A, Panitz HJ, Schubert-Frisius M, et al (2015) Dynamical downscaling of CMIP5 global circulation models over CORDEX-Africa with COSMO-CLM: evaluation over the present climate and analysis of the added value. Climate Dynamics 44(9-10):2637–2661

Dosio A, Jones RG, Jack C, et al (2019) What can we know about future precipitation in Africa? robustness, significance and added value of projections from a large ensemble of regional climate models. Climate Dynamics 53(9-10):5833–5858

Dosio A, Turner AG, Tamoffo AT, et al (2020) A tale of two futures: contrasting scenarios of future precipitation for West Africa from an ensemble of regional climate models. Environmental Research Letters 15(6):064,007

Eden JM, Widmann M, Grawe D, et al (2012) Skill, correction, and downscaling of GCM-simulated precipitation. Journal of Climate 25(11):3970–3984

Endris HS, Omondi P, Jain S, et al (2013) Assessment of the performance of CORDEX regional climate models in simulating East African rainfall. Journal of Climate 26(21):8453–8475

Ermert V, Fink AH, Jones AE, et al (2011) Development of a new version of the Liverpool malaria model. II. calibration and validation for West Africa. Malaria journal 10(1):62

Evans JL, Jaskiewicz FA (2001) Satellite-based monitoring of intraseasonal variations in tropical Pacific and Atlantic convection. Geophysical research letters 28(8):1511–1514

Ewansiha S, Singh B (2006) Relative drought tolerance of important herbaceous legumes and cereals in the moist and semi-arid regions of West Africa. Journal of Food Agriculture and Environment 4(2):188

Fiedler S, Crueger T, D'Agostino R, et al (2020) Simulated tropical precipitation assessed across three major phases of the coupled model intercomparison project (CMIP). Monthly Weather Review 148(9):3653–3680

Flato G, Marotzke J, Abiodun B, et al (2014) Evaluation of climate models. In: Climate change 2013: the physical science basis. Contribution of Working Group I to the Fifth Assessment Report of the Intergovernmental Panel on Climate Change. Cambridge University Press, p 741–866

Gidden MJ, Riahi K, Smith SJ, et al (2019) Global emissions pathways under different socioeconomic scenarios for use in CMIP6: a dataset of harmonized emissions trajectories through the end of the century. Geoscientific Model Development 12(4):1443–1475. https://doi.org/10.5194/gmd-12-1443-2019, URL https://gmd.copernicus.org/articles/12/1443/2019/

Giorgi F, Gutowski Jr WJ (2015) Regional dynamical downscaling and the CORDEX initiative. Annual Review of Environment and Resources 40:467–490

Gregory S (1983) A note on mean seasonal rainfall in the Sahel, 1931-60 and 1961-80. Geography 68(1):31–36

Hamilton H, Young G, Evans J, et al (2017) The relationship between the Guinea Highlands and the West African offshore rainfall maximum. Geophysical Research Letters 44(2):1158–1166

Hamilton H, Núñez Ocasio K, Evans J, et al (2020) Topographic influence on the African easterly jet and African easterly wave energetics. Journal of Geophysical Research: Atmospheres 125(8):e2019JD032,138

Hersbach H, Bell B, Berrisford P, et al (2020) The ERA5 global reanalysis. Quarterly Journal of the Royal Meteorological Society 146(730):1999–2049. https://doi.org/https://doi.org/10.1002/qj.3803, URL https://rmets.onlinelibrary.wiley.com/doi/abs/10.1002/qj.3803, https://arxiv.org/abs/https://rmets.onlinelibrary.wiley.com/doi/pdf/10.1002/qj.3803

Hewitson BC, Crane RG (2006) Consensus between GCM climate change projections with empirical downscaling: precipitation downscaling over South Africa. International Journal of Climatology 26(10):1315–1337. https://doi.org/10.1002/joc.1314, URL https://rmets.onlinelibrary.wiley.com/doi/abs/10.1002/joc.1314, https://arxiv.org/abs/https://rmets.onlinelibrary.wiley.com/doi/pdf/10.1002/joc.1314

Hulme M (1987) Secular changes in wet season structure in central Sudan. Journal of Arid Environments 13(1):31–46

Ibrahim B, Karambiri H, Polcher J, et al (2014) Changes in rainfall regime over Burkina Faso under the climate change conditions simulated by 5 regional climate models. Climate Dynamics 42(5):1363–1381

Issa Lélé M, Lamb PJ (2010) Variability of the intertropical front (ITF) and rainfall over the West African Sudan–Sahel zone. Journal of Climate

23(14):3984–4004

Janicot S, Thorncroft CD, Ali A, et al (2008) Large-scale overview of the summer monsoon over West Africa during the AMMA field experiment in 2006. In: Annales Geophysicae, Copernicus GmbH, pp 2569–2595

Karl TR, Nicholls N, Ghazi A (1999) Clivar/GCOS/WMO workshop on indices and indicators for climate extremes workshop summary. In: Weather and climate extremes. Springer, p 3–7

Kiladis GN, Thorncroft CD, Hall NMJ (2006) Three-dimensional structure and dynamics of African Easterly Waves. Part I: Observations. Journal of the Atmospheric Sciences 63(9):2212–2230. https://doi.org/10.1175/JAS3741.1, URL https://doi.org/10.1175/JAS3741.1, https://arxiv.org/abs/https://doi.org/10.1175/JAS3741.1

Kiviluoto K (1996) Topology preservation in self-organizing maps. In: Proceedings of International Conference on Neural Networks (ICNN'96), IEEE, pp 294–299

Koutroulis AG, Grillakis M, Tsanis I, et al (2016) Evaluation of precipitation and temperature simulation performance of the CMIP3 and CMIP5 historical experiments. Climate Dynamics 47(5):1881–1898. https://doi.org/https://doi.org/10.1007/s00382-015-2938-x

Le Barbé L, Lebel T, Tapsoba D (2002) Rainfall variability in West Africa during the years 1950–90. Journal of climate 15(2):187–202

Lebel T, Ali A (2009) Recent trends in the Central and Western Sahel rainfall regime (1990–2007). Journal of Hydrology 375(1-2):52–64

Lebel T, Diedhiou A, Laurent H (2003) Seasonal cycle and interannual variability of the Sahelian rainfall at hydrological scales. Journal of Geophysical Research: Atmospheres 108(D8)

Lebel T, Cappelaere B, Galle S, et al (2009) AMMA-CATCH studies in the Sahelian region of West-Africa: An overview. Journal of Hydrology 375(1-2):3–13

Liebmann B, Bladé I, Bond NA, et al (2008) Characteristics of North American summertime rainfall with emphasis on the monsoon. Journal of Climate 21(6):1277–1294

Maranan M, Fink AH, Knippertz P, et al (2019) Interactions between convection and a moist vortex associated with an extreme rainfall event over southern West Africa. Monthly Weather Review 147(7):2309–2328

Maraun D, Wetterhall F, Ireson A, et al (2010) Precipitation downscaling under climate change: Recent developments to bridge the gap between dynamical models and the end user. Reviews of geophysics 48(3)

Mathon V, Laurent H, Lebel T (2002) Mesoscale convective system rainfall in the Sahel. Journal of applied meteorology 41(11):1081–1092

Mera R, Laing AG, Semazzi F (2014) Moisture variability and multiscale interactions during spring in West Africa. Monthly Weather Review 142(9):3178–3198

Mortimore M (2010) Adapting to drought in the Sahel: lessons for climate change. Wiley interdisciplinary reviews: climate change 1(1):134–143

National Climatic Data Center (2020) Global summary of day. URL https://catalog.data.gov/dataset/global-surface-summary-of-the-day-gsod

Nguyen H, Thorncroft CD, Zhang C (2011) Guinean coastal rainfall of the West African monsoon. Quarterly Journal of the Royal Meteorological Society 137(660):1828–1840

Niang I, Ruppel O, Abdrabo M, et al (2014) Africa. In: Barros V, Field C, Dokken D, et al (eds) Climate Change 2014: Impacts, Adaptation, and Vulnerability. Part B: Regional Aspects. Contribution of Working Group II to the Fifth Assessment Report of the Intergovernmental Panel on Climate Change. Cambridge University Press, Cambridge, chap 22, p 1199–1265

Nicholson SE (1993) An overview of African rainfall fluctuations of the last decade. Journal of climate pp 1463–1466

Nicholson SE (2013) The West African Sahel: A review of recent studies on the rainfall regime and its interannual variability. International Scholarly Research Notices 2013

Núñez Ocasio KM, Evans JL, Young GS (2020) Tracking mesoscale convective systems that are potential candidates for tropical cyclogenesis. Monthly Weather Review 148(2):655–669

Paeth H, Capo-Chichi A, Endlicher W (2008) Climate change and food security in tropical West Africa—a dynamic-statistical modelling approach. Erdkunde pp 101–115

Paeth H, Hall NM, Gaertner MA, et al (2011) Progress in regional downscaling of West African precipitation. Atmospheric science letters 12(1):75–82

Panthou G, Vischel T, Lebel T (2014) Recent trends in the regime of extreme rainfall in the Central Sahel. International Journal of Climatology 34(15):3998–4006

Parham PE, Michael E (2010) Modeling the effects of weather and climate change on malaria transmission. Environmental health perspectives 118(5):620–626

Perkins SE, Pitman A, Holbrook N, et al (2007) Evaluation of the AR4 climate models' simulated daily maximum temperature, minimum temperature, and precipitation over australia using probability density functions. Journal of climate 20(17):4356–4376. https://doi.org/https://doi.org/10.1175/JCLI4253.1

Polasky AD, Evans JL, Fuentes JD, et al (2021) Statistical climate model downscaling for impact projections in the Midwest United States. International Journal of Climatology

Roehrig R, Bouniol D, Guichard F, et al (2013) The present and future of the West African monsoon: A process-oriented assessment of CMIP5 simulations along the AMMA transect. Journal of Climate 26(17):6471–6505

Rose BE, Lin CA (2003) Precipitation from vertical motion: a statistical diagnostic scheme. International Journal of Climatology: A Journal of the Royal Meteorological Society 23(8):903–919

Rybka H, Tost H (2014) Uncertainties in future climate predictions due to convection parameterisations. Atmospheric Chemistry and Physics 14(11):5561–5576

Schlenker W, Lobell DB (2010) Robust negative impacts of climate change on African agriculture. Environmental Research Letters 5(1):014,010

Sillmann J, Kharin V, Zhang X, et al (2013) Climate extremes indices in the CMIP5 multimodel ensemble: Part 1. model evaluation in the present climate. Journal of Geophysical Research: Atmospheres 118(4):1716–1733

Sinha P, Mann ME, Fuentes JD, et al (2018) Downscaled rainfall projections in south Florida using self-organizing maps. Science of The Total Environment 635:1110 – 1123. https://doi.org/https://doi.org/10.1016/j.scitotenv.2018.04.144

Stefanova L, Misra V, Chan S, et al (2012) A proxy for high-resolution regional reanalysis for the Southeast United States: assessment of precipitation variability in dynamically downscaled reanalyses. Climate dynamics 38:2449–2466

Stephens GL, L'Ecuyer T, Forbes R, et al (2010) Dreary state of precipitation in global models. Journal of Geophysical Research: Atmospheres 115(D24). https://doi.org/https://doi.org/10.1029/2010JD014532

Stern RD, Dennett MD, Garbutt DJ (1981) The start of the rains in West Africa. Journal of Climatology 1(1):59–68

Sultan B, Gaetani M (2016) Agriculture in West Africa in the twenty-first century: Climate change and impacts scenarios, and potential for adaptation. Frontiers in Plant Science 7. https://doi.org/10.3389/fpls.2016.01262, URL https://www.frontiersin.org/article/10.3389/fpls.2016.01262

Sultan B, Janicot S (2003) The West African monsoon dynamics. part II: The "preonset" and "onset" of the summer monsoon. Journal of climate

16(21):3407–3427

Sylla MB, Nikiema PM, Gibba P, et al (2016) Climate change over West Africa: Recent trends and future projections. Adaptation to climate change and variability in rural West Africa pp 25–40

Thorncroft C, Blackburn M (1999) Maintenance of the African easterly jet. Quarterly Journal of the Royal Meteorological Society 125(555):763–786

Thorncroft C, Hoskins B (1994) An idealized study of African easterly waves. I: A linear view. Quarterly Journal of the Royal Meteorological Society 120(518):953–982

Thorncroft CD, Hall NM, Kiladis GN (2008) Three-dimensional structure and dynamics of African easterly waves. part III: Genesis. Journal of the Atmospheric Sciences 65(11):3596–3607

Thorncroft CD, Nguyen H, Zhang C, et al (2011) Annual cycle of the West African monsoon: regional circulations and associated water vapour transport. Quarterly Journal of the Royal Meteorological Society 137(654):129–147

Todorov A (1985) Sahel: the changing rainfall regime and the "Normals" used for its assessment. Journal of climate and Applied Meteorology pp 97–107

Vizy EK, Cook KH, Crétat J, et al (2013) Projections of a wetter Sahel in the twenty-first century from global and regional models. Journal of climate 26(13):4664–4687

World Bank (2020) Healthstats population estimates and projections database. Online, URL https://databank.

worldbank.org/source/health-nutrition-and-population-statistics:-population-estimates-and-projections

Xue Y, De Sales F, Lau WM, et al (2010) Intercomparison and analyses of the climatology of the West African Monsoon in the West African Monsoon Modeling and Evaluation project (WAMME) first model intercomparison experiment. Climate Dynamics 35(1):3–27

Zhuang J, Dussin R, Jüling A, et al (2020) xesmf: v0.3.0. https://doi.org/https://doi.org/10.5281/zenodo.3700105